Effects of entrance channel and compound nucleus in the fusion cross sections for $^{28}Si+^{28}Si$, $^{16}O+^{40}Ca$, $^{32}S+^{30}Si$, and $^{12}C+^{50}Cr$

Y. Nagashima, J. Schimizu, T. Nakagawa, Y. Fukuchi, W. Yokota, K. Furuno, M. Yamanouchi, S. M. Lee, N. X. Dai,* and T. Mikumo
Institute of Physics and Tandem Accelerator Center, University of Tsukuba, Ibaraki 305, Japan

T. Motobayashi
Department of Physics, Rikkyo University, Tokyo, Japan
(Received 19 April 1985)

In order to study the physics responsible for a limitation in angular momentum in heavy-ion fusion reactions, fusion cross sections for the reactions $^{28}Si+^{28}Si$, $^{16}O+^{40}Ca$, $^{32}S+^{30}Si$, and $^{12}C+^{50}Cr$ have been measured at several incident energies covering lower and higher energy regions by detecting the yields of the fusion-evaporation residues. The limiting angular momenta for fusion are extracted from the measured fusion cross sections and compared with calculations based upon several models. Through the systematic study of different entrance channels forming the same compound nucleus, a strong entrance channel effect has been observed for very asymmetric systems. Our conclusion is that the entrance channel is significant in limiting the fusion cross section in the higher energy region.

I. INTRODUCTION

In order to understand the gross features of heavy-ion reaction mechanisms, the study of the fusion reaction is very crucial since it is not only one of the elemental processes by itself, but also is intimately related to many other reaction mechanisms.[1] Although in the last decades many experimental and theoretical efforts have been focused on the fusion reaction and various models have been proposed,[2–18] a good understanding of the fusion mechanism has not yet been achieved. In this situation, the present study is intentionally focused on several particular cases of fusion reactions where the predictions of theoretical models differ appreciably.

The heavy-ion fusion process is generally considered to account entirely for the process of compound nucleus (CN) formation, especially at low incident energies, as the contribution from compound elastic scattering is very small. Since evaporation is the dominant decay mode for compound nucleus formation in the case of $A_{CN} < 100$, it is sufficient in the present study to measure the cross section of evaporation residues to determine the fusion cross section: $\sigma_{fus} = \sigma_{fus-ER}$.

In a sharp cutoff approximation, the total reaction cross section σ_{reac} and the fusion cross section σ_{fus} are expressed as follows:

$$\begin{aligned}\sigma_{reac} &= (\pi\hbar^2/2\mu E_{c.m.}) \sum^{L_{max}} (2L+1) \\ &= (\pi\hbar^2/2\mu E_{c.m.})(L_{max}+1)^2 , \\ \sigma_{fus} &= (\pi\hbar^2/2\mu E_{c.m.}) \sum^{L_{fus}} (2L+1) \\ &= (\pi\hbar^2/2\mu E_{c.m.})(L_{fus}+1)^2 ,\end{aligned} \tag{1}$$

where μ is the reduced mass and $E_{c.m.}$ is the energy in the center-of-mass system.

Through the systematic study of fusion cross sections, it has been realized that σ_{fus} exhibits a simple dependence on $E_{c.m.}^{-1}$ and can be divided into three energy regions $\sigma_{fus}^{(I)}$, $\sigma_{fus}^{(II)}$, and $\sigma_{fus}^{(III)}$ as is shown schematically in Fig. 1. In the low energy region, $\sigma_{fus}^{(I)}$ exhausts almost the entire total reaction cross section σ_{reac} for light-light (LL) systems, while in the intermediate energy region, $\sigma_{fus}^{(II)}$ starts to deviate markedly from σ_{reac}, and finally $\sigma_{fus}^{(III)}$ decreases at high energies.

In region II, $\sigma_{fus}^{(II)}$ is usually smaller than σ_{reac} and L_{fus} is smaller than L_{max}. Thus, we get $\sigma_{fus}^{(II)}$ as

$$\sigma_{fus}^{(II)} = (\pi\hbar^2/2\mu E_{c.m.})(L_{fus}+1)^2 . \tag{2}$$

There are at least two alternative ideas to explain the physical origin of the behavior of σ_{fus} in region II; the entrance channel effect[2–7,10–12] and the compound nucleus effect.[9,16,17]

The idea of the entrance channel effect is that the complete fusion cross section is limited by the disappearance

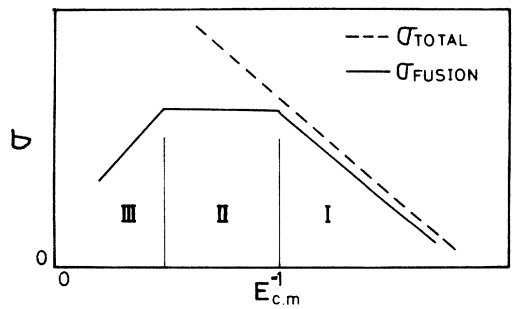

FIG. 1. Schematic drawing for the fusion cross section and the total reaction cross section plotted versus the inverse of $E_{c.m.}$.

of an L pocket, the existence of a limiting trajectory, or by a critical distance in the entrance channel. Several models such as the critical distance model,[2,3] the friction model,[11] and the Bass model[5–7] are based on this idea. On the other hand, the fusion cross section might be limited by a critical angular momentum (L_{cr}) related to the yrast line of the compound nucleus, that is, $\sigma_{fus}^{(II)}$ is restricted by properties of the compound nucleus itself. The statistical yrast line model[16] and the level density model[17] fall into this category.

The experimental data are sometimes equally well reproduced by alternative models, and those models are only partially successful. In order to investigate the physics of fusion in region II, we have studied the behavior of fusion cross sections for symmetric and asymmetric systems forming the same compound nucleus; $^{28}Si+^{28}Si$ and $^{16}O+^{40}Ca$ leading to the CN ^{56}Ni, and $^{32}S+^{30}Si$ and $^{12}C+^{50}Cr$ leading to the CN ^{62}Zn. It should be mentioned that the ratios of projectile to target masses vary much more markedly than those covered in the previous studies.

II. EXPERIMENTAL METHOD

The main parts of the experiment were performed at the Tandem Accelerator Center of the University of Tsukuba (UTTAC). Measurements for the $^{12}C+^{50}Cr$ system at higher energies were done at the Research Center for Nuclear Physics at the University of Osaka (RCNP).

Ions of ^{28}Si, ^{32}S, ^{16}O, and ^{12}C from a sputter ion source (TUNIS) (Ref. 19) were accelerated by a 12 MV tandem van de Graaff accelerator.[20] The size of the beam spot on the target was confined to 1.8 mm in diameter by a collimator system in front of the target. The most forward angle accessible to the measurement of fusion-evaporation residues was estimated to be about 1.7°.

Thin self-supporting $^{28}SiO_2$ (150 $\mu g/cm^2$) and $^{30}SiO_2$ (100 $\mu g/cm^2$) targets were used for the fusion cross section measurements of the systems $^{28}Si+^{28}Si$ and $^{32}S+^{30}Si$, respectively. Targets of ^{40}Ca (50 $\mu g/cm^2$) were evaporated on carbon foil (10 $\mu g/cm^2$). To avoid oxidation, ^{40}Ca targets were treated under argon gas. The oxygen contamination in this target was checked to be less than a few

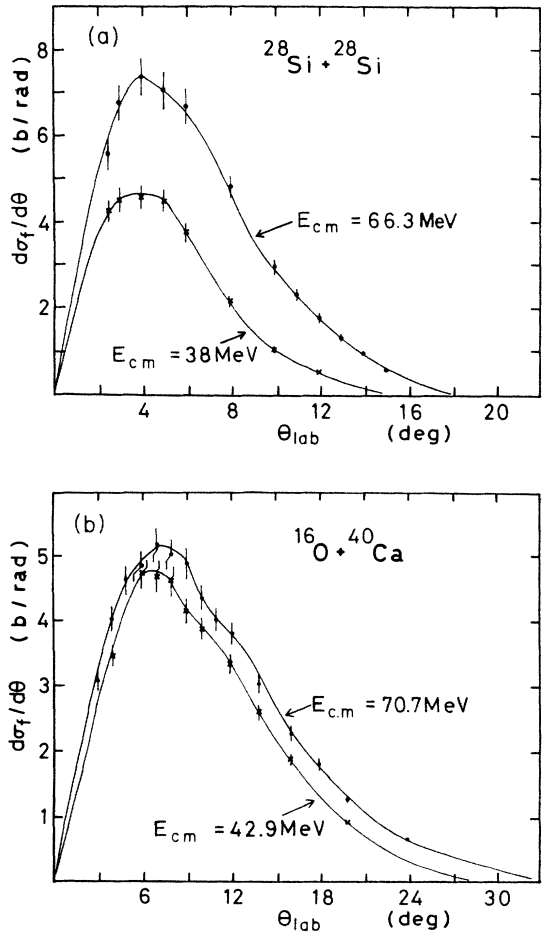

FIG. 2. (a) Angular distributions $d\sigma_{fus}/d\Omega$ of the evaporation residues from the reaction $^{28}Si+^{28}Si$. (b) Angular distributions $d\sigma_{fus}/d\Omega$ of the evaporation residues from the reaction $^{16}O+^{40}Ca$. The solid line is to guide the eye.

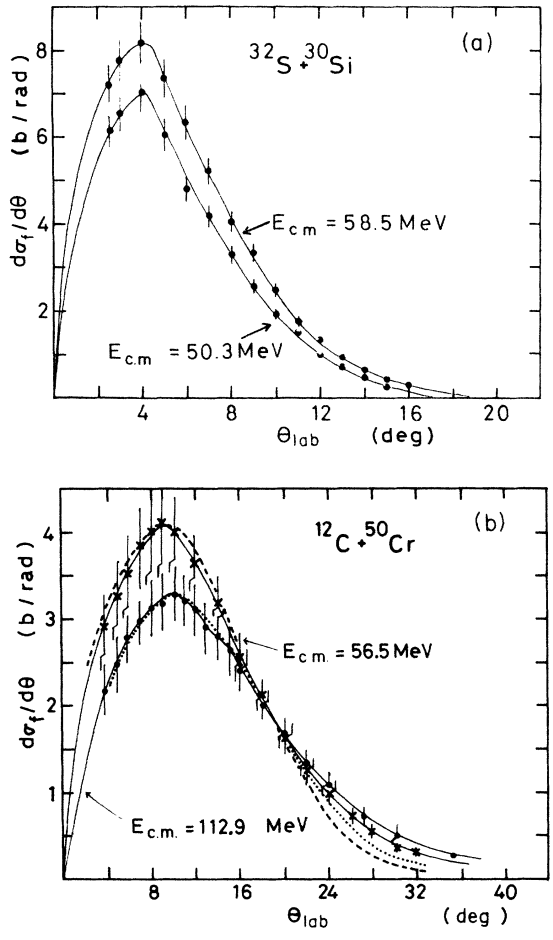

FIG. 3. (a) Angular distributions $d\sigma_{fus}/d\Omega$ of the evaporation residues from the reaction $^{32}S+^{30}Si$. (b) Angular distributions $d\sigma_{fus}/d\Omega$ of the evaporation residues from the reaction $^{12}C+^{50}Cr$. The solid line is to guide the eye. The broken line and the dotted line are the calculation by the RECOIL program code.

percent by elastic scattering. A self-supporting enriched ^{50}Cr foil (125 μg/cm^2) was used for the measurement of ^{12}C+^{50}Cr.

Two sets of gas-ΔE semiconductor-E counter telescopes[21] were used. Isobutane gas was used in a flow mode and maintained at a constant pressure (2–15±0.1 Torr). No appreciable gain shift of pulses from the gas counter was observed during the experiment.

The ^{12}C+^{50}Cr experiment at higher energies was performed at the AVF cyclotron laboratory at RCNP. The scattering chamber setup was almost identical to that at UTTAC except for the beam collimator and monitors. Two monitors were set at symmetrical positions viewed from the beam path ($\theta=\pm5°$, $\phi=3°$), in order to detect the fluctuations of the beam spot on the target. The deviations were small during continuous operation of the ion source. We used the same ^{50}Cr target, gas counters, gas flow systems, and electronic circuits as those used for the experiments at UTTAC.

The differential fusion cross section for a particular system ($d\sigma/d\Omega$) has been derived from the accumulated yield of evaporation residues. The yield of elastic scattering detected by the fixed monitor counter was used for the relative normalization. The absolute value of the differential fusion cross section ($d\sigma/d\Omega$) was determined by normalizing the fusion yield to the elastic scattering measured simultaneously with the evaporation residues. The differential angular distributions were extrapolated from 2.5° to 0° by a smooth curve and also extrapolated to backward angles by an exponentially decaying curve. The interpolations between data points were done by a smooth curve as shown in Figs. 2 and 3. The overall errors for the ^{28}Si+^{28}Si, ^{32}S+^{30}Si, ^{16}O+^{40}Ca, and ^{12}C+^{50}Cr systems were estimated to be ±10%, ±10%, ±9%, and ±16%, respectively.

III. RESULTS

Typical two-dimensional plots of ΔE-E measurements are shown in Figs. 4 and 5. The separation of the evaporation residues from the other yields is sufficient for clear identification. In the maps for ^{28}Si+^{28}Si, ^{32}S+^{30}Si, and ^{16}O+^{40}Ca, the data are characterized by three elemental regions. The lowest part is due to elements of the beams because the position of the rejected elastic scattering in these maps is just located on this locus. The middle part is due to ejectiles from O or C included in the target. The uppermost parts are due to the evaporation residues in question. On the other hand, we see only two parts of yields in the ^{12}C+^{50}Cr case, as the target was a self-supporting ^{50}Cr foil. The energy spectra of the evaporation residues extracted from the two-dimensional map are also shown in Figs. 4 and 5.

Figures 6 and 7 show typical examples for the elastic cross sections divided by the Rutherford or Mott cross sections $\sigma(\theta)_{el}/\sigma(\theta)_{Ruth}$. These ratios at the most forward angles are equal to 1 in all systems.

Complete angular distributions ($\theta_{lab}\cong2.5°$–30°) for the evaporation residues were measured at each energy point. Figures 2 and 3 show typical angular distributions for each system. The solid lines are guides for the eye. The

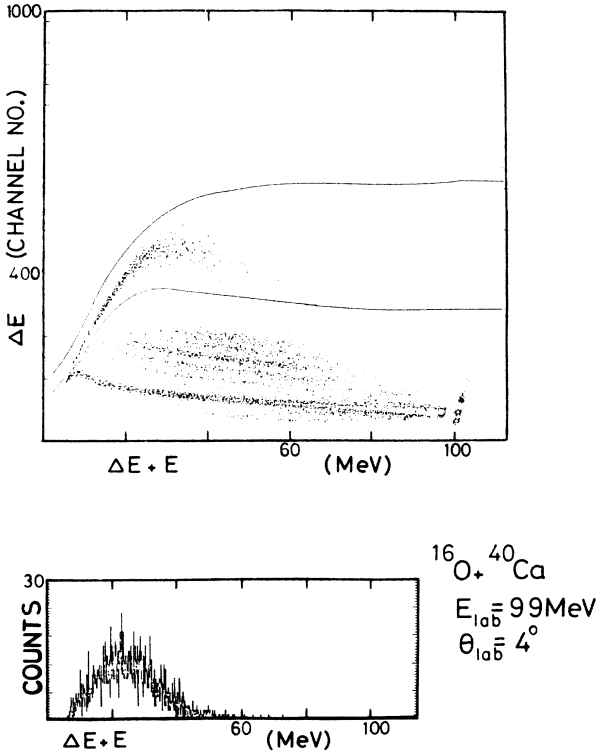

FIG. 4. Yield distribution in the $\Delta E+E$ and ΔE plane for ^{16}O+^{40}Ca at $\theta_{lab}=4°$, $E_{lab}=99$ MeV. The projected energy spectrum of the yield is between the two lines.

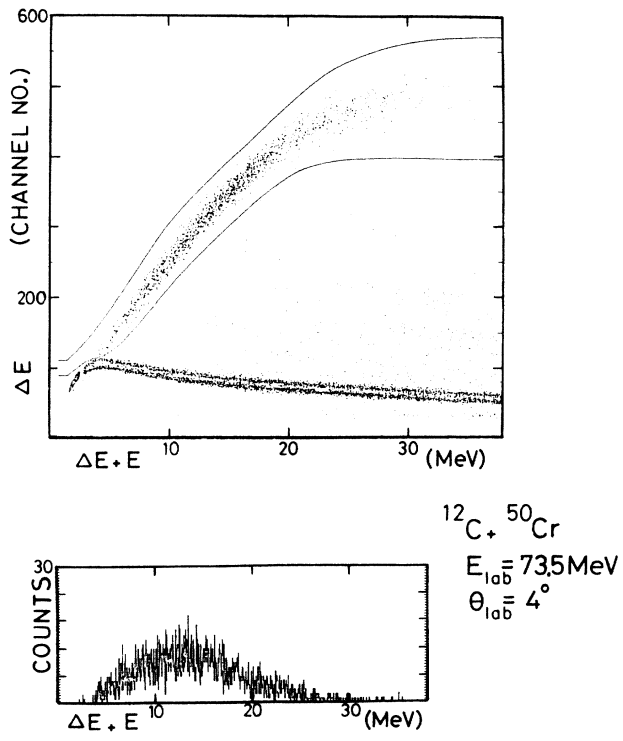

FIG. 5. Yield distribution in the $\Delta E+E$ and ΔE plane for ^{12}C+^{50}Cr at $\theta_{lab}=4°$, $E_{lab}=73.5$ MeV. The projected energy spectrum of the yield is between the two lines.

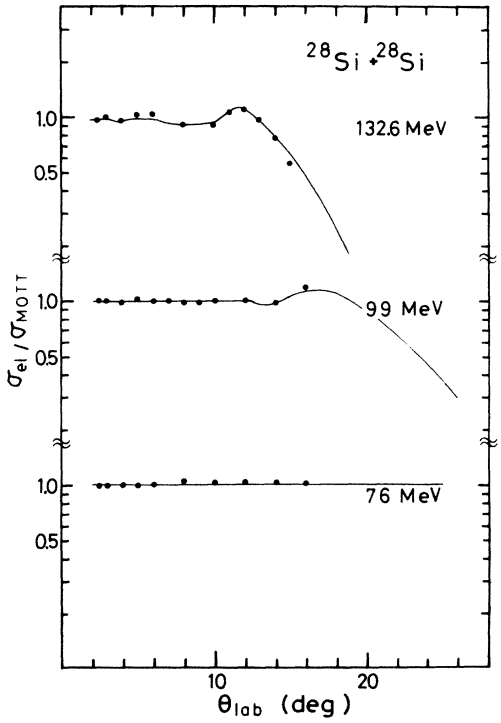

FIG. 6. Angular distributions $\sigma_{el}/\sigma_{Mott}$ for the elastic scattering divided by the Mott scattering for $^{28}Si+^{28}Si$.

angular distribution $d\sigma/d\theta$ of evaporation residues usually peaks at very forward angles $\theta_{peak}=4°-10°$. The peak, however, shifts to a more backward angle as the incident energy increases, which is understood as being due to an increase in the number of evaporated particles. Consequently the distribution broadens and the multiplication of $d\sigma/d\Omega$ with $\sin\theta$ results in a shift of the peak in $d\sigma/d\theta$.

The total fusion cross sections deduced from the experiments are listed in Table I and are shown graphically in Figs. 8 and 9. The slopes of the fusion cross sections for $^{28}Si+^{28}Si$, $^{16}O+^{40}Ca$, and $^{32}S+^{30}Si$ have a bending point at $E^{-1}_{c.m.}=0.020$, 0.020, and 0.017, respectively. The fusion cross section of $^{28}Si+^{28}Si$, $^{16}O+^{40}Ca$, and $^{32}S+^{30}Si$ at this point is about 1100 mb, 1230 mb, and 1050 mb, respectively.

The critical angular momenta (L_{cr}) obtained from the fusion cross sections by using Eqs. (2) are also listed in Table I and are plotted in the plane of the compound excitation energy (E^*) vs $J(J+1)$. Figures 10 and 11 show these results. It appears that the more asymmetric a system is the more it deviates from the yrast line.

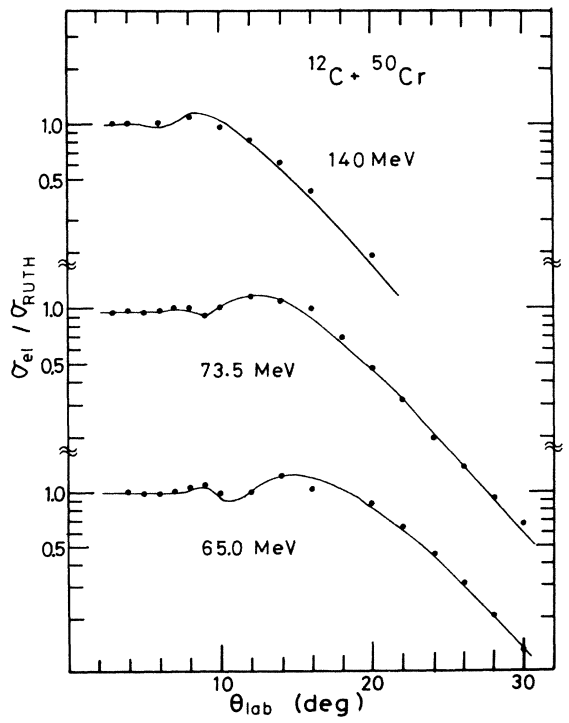

FIG. 7. Angular distributions $\sigma_{el}/\sigma_{Ruth}$ for the elastic scattering divided by the Rutherford scattering for $^{12}C+^{50}Cr$.

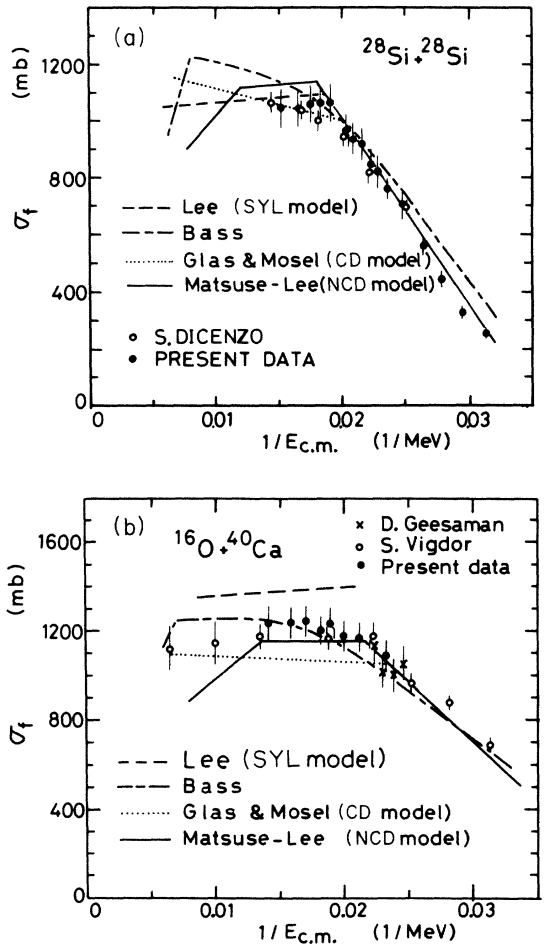

FIG. 8. Experimental and theoretical fusion cross sections for $^{28}Si+^{28}Si$ (a) and for $^{16}O+^{40}Ca$ (b) vs $1/E_{c.m.}$. Closed circles, results of the present study; open circles from Refs. 22 (a) and 24 (b); crosses from Ref. 23. For comparison are shown theoretical cross sections obtained using various models (long dashed line from Ref. 16, dashed-short-dashed line from Ref. 6, dotted line from Ref. 3, and solid line from Ref. 18).

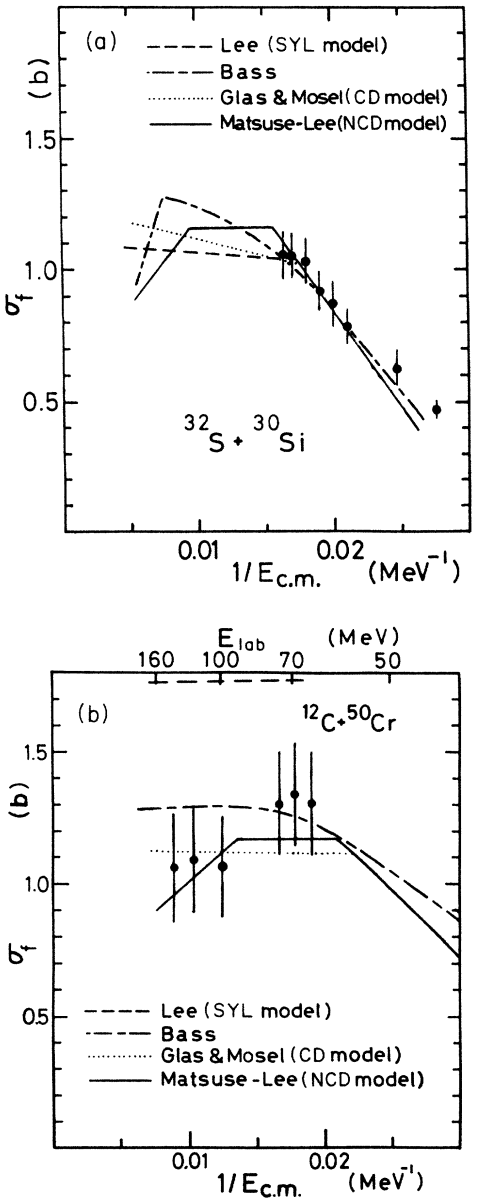

FIG. 9. Experimental and theoretical fusion cross sections for $^{32}S+^{30}Si$ (a) and for $^{12}C+^{50}Cr$ (b) vs $1/E_{c.m.}$. Closed circles, results of the present study. For comparison are shown theoretical cross sections obtained using various models (long dashed line from Ref. 16, dashed-short-dashed line from Ref. 6, dotted line from Ref. 3, and solid line from Ref. 18).

IV. DISCUSSION

In this section, we will first describe the theoretical models which will be frequently used for comparison with our data: the critical distance model,[2,3] the Bass model,[5–7] the statistical yrast line model,[16] and a new critical distance model[18] for the higher incident energy region. Then, we discuss specifically the present results for $^{28}Si+^{28}Si$ and $^{16}O+^{40}Ca$, and those of $^{32}S+^{30}Si$ and $^{12}C+^{50}Cr$, and finally the marked difference found in σ_{fus} for $^{32}S+^{30}Si$ and for $^{12}C+^{50}Cr$ will be elaborated in detail.

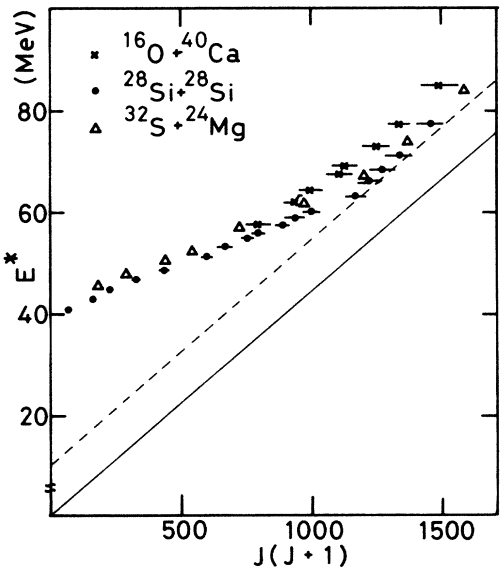

FIG. 10. Critical angular momenta L_{cr} derived from the experimental fusion cross sections are shown in the plane of the excitation energy E^* vs $J(J+1)$, where J denotes the total angular momentum of the compound nucleus ^{56}Ni. The solid line represents the yrast line of ^{56}Ni and is calculated with the rigid-body moment of inertia. The statistical yrast line is shown by the dashed line.

The critical distance model introduces a critical distance R_{cr} as a condition for fusion to take place.[2,3] Once there exists R_{cr} for a given system, then the partial waves greater than the critical angular momentum L_{cr} cannot

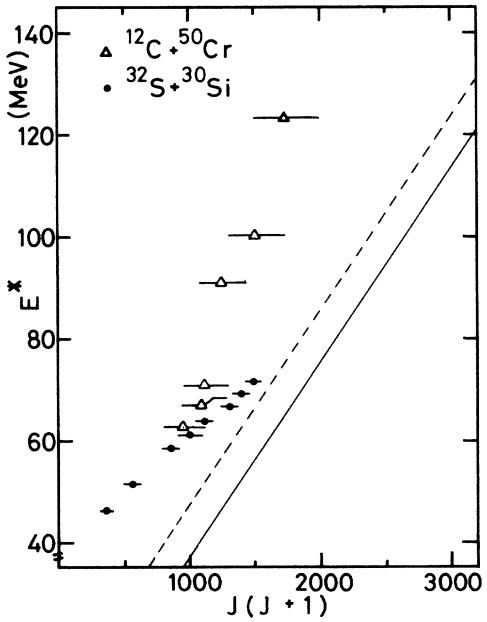

FIG. 11. Critical angular momenta L_{cr} derived from the experimental fusion cross sections are shown in the plane of the excitation energy E^* vs $J(J+1)$, where J denotes the total angular momentum of the compound nucleus ^{62}Zn. The solid line represents the yrast line of ^{62}Zn and is calculated with the rigid-body moment of inertia. The statistical yrast line is shown by the dashed line.

TABLE I. The measured fusion cross section as a function of bombarding energy.

Systems	$E_{c.m.}$ (MeV)	E^* (MeV)	σ_{fus} (mb)	L_{fus} (h)
$^{28}Si+^{28}Si$	66.3	77.2	1050±69	37.5±1.3
	60.5	71.4	1058±45	35.9±1.3
	57.5	68.4	1064±70	35.1±1.2
	55.0	65.9	1068±69	34.3±1.2
	52.5	63.4	1072±70	33.6±1.2
	49.5	60.4	970±63	31.0±1.0
	48.0	58.9	938±61	30.0±1.0
	46.5	57.4	922±60	29.2±1.0
	45.0	55.9	852±56	27.6±0.9
	44.0	54.9	828±54	26.9±0.9
	42.5	53.4	765±36	25.3±0.9
	40.5	51.4	715±47	23.9±0.8
	38.0	48.9	562±37	20.3±0.8
	36.0	46.9	446±29	17.5±0.6
	34.0	44.9	330±22	14.5±0.5
	32.0	42.9	260±17	12.3±0.5
	30.0	40.9	115±8	7.6±0.4
$^{16}O+^{40}Ca$	70.7	85.0	1241±73	38.0±1.2
	62.9	77.2	1245±74	35.9±1.1
	58.6	72.9	1250±74	34.7±1.1
	55.0	69.3	1205±71	33.0±1.0
	52.9	67.2	1239±74	32.8±1.0
	50.0	64.3	1183±70	31.1±1.0
	47.1	61.4	1173±70	30.0±1.0
	42.9	57.2	1097±65	27.6±1.0
$^{32}S+^{30}Si$	61.0	71.7	1055±69	38.0±1.3
	58.5	69.2	1051±68	37.0±1.3
	55.7	66.4	1033±67	35.8±1.2
	53.2	63.9	915±60	32.9±1.0
	50.3	61.0	876±90	31.2±1.7
	47.9	58.6	783±65	28.7±1.3
	40.6	51.3	622±70	23.4±1.4
	36.2	46.9	463±30	18.9±0.7
$^{12}C+^{50}Cr$	112.9	123.8	1062±165	41.0±3.1
	96.8	107.0	1076±165	38.2±2.8
	80.6	91.5	1059±165	34.5±2.5
	59.3	70.2	1316±210	32.9±2.5
	56.5	67.4	1352±210	32.7±2.4
	52.4	63.3	1313±210	30.8±2.4

form the fused system. This condition is

$$E_{c.m.}=V(R_{cr})+(\pi\hbar^2/2\mu R_{cr}^2)L_{cr}(L_{cr}+1)\ . \tag{3}$$

Combining Eqs. (2) and (3), σ_{fus} becomes as follows:

$$\sigma_{fus}=\pi R_{cr}^2[1-V(R_{cr})/E_{c.m.}]\ . \tag{4}$$

From systematic studies, Galin *et al.*[2] have found the value of $r_{cr}=1.00\pm0.07$, and for $V(R_{cr})$, Ngo *et al.*[25] proposed a suitable formula. The main virtue of this model is its simplicity and applicability for a certain range of mass systems.

The Bass model is one of the classical potential models which is derived from the liquid drop model. This model explains the limiting angular momentum for fusion as follows:

$$L_{fus}^2=\frac{(1-x)[(E_{c.m.}-E_1)(1-f^2)+(E_2-E_1)f^2]}{2yf^2(E_2-E_1)}$$

$$E_1<E_{c.m.}<E_2\ ,$$

$$L_{fus}^2=\frac{1-x}{2f^2y}\quad E_{c.m.}>E_2\ ,$$

where x, y, and f are dimensionless parameters (see Ref. 6). The critical energy E_i $(i=1,2)$ is

$$\frac{Z_1Z_2e^2}{R_{12}}\left[1+\frac{1-x}{2kx}-\frac{1.35}{xR_{12}}\right]\ \text{MeV}\ ,$$

($k=1$ for $i=1$, $k=f^2$ for $i=2$), where Z_1 is the atomic number of the projectile, Z_2 is the atomic number of the

target, and R_{12} is the sum of the half-density matter radii. At energies below E_1, $L_{\rm fus}$ is determined by the condition that the $E_{\rm c.m.}$ must be equal to the maximum of the corresponding potential $V(L)$.

An alternative model suggests that $\sigma_{\rm fus}$ might be limited by the properties of the CN.[16,17] Lee *et al.* have proposed the statistical yrast line model,[16] assuming the existence of a fusion limiting line in the CN. The statistical yrast line and $\sigma_{\rm fus}$ are given by

$$E_{\rm SY}=\hbar^2 J(J+1)/2I+\Delta Q\ , \tag{5}$$

$$\sigma_{\rm fus}=(I/\mu)[1+(Q-\Delta Q)/E_{\rm c.m.}]\ , \tag{6}$$

where Q is the separation energy of the entrance channel from the compound nucleus. This model can account rather well for systems up to $A=A_1+A_2<80$, but a theoretical foundation is not yet given. There is an attempt based on the averaged S-matrix approach.[26] A different approach is based upon a limitation due to the level density in the CN postulating the condition of $(\Gamma_{\rm tot}/D)_J\geq 1$ in the CN.[17]

Matsuse *et al.* have recently proposed a new concept of the critical distance in the high energy region.[18] In this model two critical distances which are $D_{\rm III}=\langle d^2\rangle^{1/2}$ and $D_{\rm II}=2^{1/2}D_{\rm III}$ are introduced, where $\langle d^2\rangle$ is assumed to be the mean square distance between the two nuclei A_1 and A_2, i.e.,

$$A\langle r^2\rangle_A=A_1\langle r^2\rangle_{A1}+A_2\langle r^2\rangle_{A2}+(A_1A_2/A)\langle d^2\rangle\ , \tag{7}$$

where $A=A_1+A_2$. According to this model, $\sigma_{\rm fus}$ in the higher energy region can be expressed analogous to Eq. (4) as

$$\sigma_{\rm fus}^{(j)}=\pi D_j^2[1-V(D_j)/E_{\rm c.m.}]\ ,\quad j={\rm II\ and\ III}\ , \tag{8}$$

where the nuclear part (V_n) of the potential (V) is given as follows:

$$V_n(r)=\mu\omega_d^2 r^2/2-\mu\omega_d^2\langle d^2\rangle-Q\quad r<D_{\rm III}\ , \tag{9}$$

$$=X_1 e^{-(r-D_{\rm III})/r_1}+X_2 e^{-(r-D_{\rm III})/r_2}$$

$$D<r<D_{\rm II}\ , \tag{10}$$

where $\omega_d=\beta\omega$, $\hbar\omega=40A^{-1/3}$, $r_1=D_{\rm III}/f_1$, $r_2=D_{\rm III}/2f_0$, $f=r_0+f_1 D_{\rm III}Y^2$, and $Y=|A_1-A_2|/(A_1+A_2)$. β, f_0, and f_1 are fixed to 0.675, 3.5, and 0.35, respectively.

A. Discussion of the ^{28}Si+^{28}Si and ^{16}O+^{40}Ca systems

The dotted lines in Fig. 8 are the calculations of $\sigma_{\rm fus}^{\rm (II)}$ by the critical distance model. The parameter r_c is fixed to be 1.00 fm, as given by Galin *et al.*,[2] and for $V_{\rm cr}(R_{\rm cr})$ the empirical potential values[25] are used. Although the experimental $\sigma_{\rm fus}^{\rm (II)}$ for ^{28}Si+^{28}Si are well reproduced by the critical distance model, the ^{16}O+^{40}Ca data are not: at $E_{\rm c.m.}=65$ MeV the deviation is about 200 mb, well outside the experimental error. This discrepancy may come from the fact that closed shell nuclei like ^{16}O and ^{40}Ca may affect a critical distance as discussed by Glas and Mosel.[3]

The calculations by the Bass model are shown with the chain lines in Fig. 8. The agreement between data and calculations for both systems is fairly good.

The broken lines in Fig. 8 are calculated by the statistical yrast line model.[16] The agreement between the data and the calculation for ^{28}Si+^{28}Si is fairly good. In the case of ^{16}O+^{40}Ca, however, calculated cross sections are systematically larger than the experimental values by about 150 mb.

The solid lines in Fig. 8 are calculated by the new critical distance model.[18] In region II the agreement with both systems is fairly good. It appears that the entrance channel effect gives a better account of the $\sigma_{\rm fus}$ limitation in region II than the compound nucleus one for asymmetric systems.

The critical angular momenta $L_{\rm fus}$ for ^{28}Si+^{28}Si, ^{16}O+^{40}Ca, and ^{32}S+^{24}Mg,[27] deduced from the experimental fusion cross sections by the use of Eq. (2), are shown in Fig. 10. The solid line exhibits the yrast line of the CN ^{56}Ni with $r_0=1.2$ fm. The dashed line shows the statistical yrast line. As can be seen from Fig. 10, $L_{\rm fus}$ values of ^{28}Si+^{28}Si follow the statistical yrast line, while those of ^{32}S+^{24}Mg show small deviations of E^* by about 3 MeV and those of ^{16}O+^{40}Ca do show larger systematic deviations of E^* by about 8 MeV. When we consider the magnitude of the error, it is difficult to reach a conclusion. However, an entrance channel effect might be present. This feature is more obvious in the case of ^{32}S+^{30}Si and ^{12}C+^{50}Cr.

B. Discussion of the ^{32}S+^{30}Si and ^{12}C+^{50}Cr systems

The excitation function of the fusion cross section for ^{32}S+^{30}Si is shown in Fig. 9(a) and that for ^{12}C+^{50}Cr in Fig. 9(b).

The dotted lines in Fig. 9 again are calculated by the critical distance model with the same set of parameters as those used for ^{28}Si+^{28}Si and ^{16}O+^{40}Ca. Though the average values of the calculated $\sigma_{\rm fus}^{\rm (II)}$ agree with the experimental $\sigma_{\rm fus}^{\rm (II)}$ for ^{12}C+^{50}Cr within the limit of errors, the trend of $\sigma_{\rm fus}^{\rm (II)}$ is not well reproduced.

The calculations by the Bass model are shown with chained lines in Fig. 9. Though the absolute values are larger, the trend is similar and the agreement with the experimental values is rather good.

The broken lines in Fig. 9 are calculated by the statistical yrast line model with the same set of parameters as for the other systems. It appears that the $\sigma_{\rm fus}^{\rm (II)}$ for ^{32}S+^{30}Si does not contradict at least the model prediction. However, a striking contrast is to be seen in $\sigma_{\rm fus}^{\rm (II)}$ for ^{12}C+^{50}Cr. The $\sigma_{\rm fus}^{\rm (II)}$ calculated by the statistical yrast line model at the top of Fig. 9(b) are much larger than the experimental data, and the deviations are beyond the experimental errors. This fact clearly indicates that the entrance channel of ^{12}C+^{50}Cr plays a decisive role in the fusion cross section at higher energies. The situation is more clearly demonstrated if we plot the critical angular momenta of ^{12}C+^{50}Cr and those of ^{32}S+^{30}Si in the E^* vs $J(J+1)$ plane of the ^{62}Zn compound nucleus (Fig. 11). The critical angular momenta of ^{32}S+^{30}Si are approaching the statistical yrast line, while those of ^{12}C+^{50}Cr deviate more and more at higher $J(J+1)$.

In order to explain the entrance channel effect, which is a striking feature in our present experiment of fusion reactions leading to the same compound system, an attempt has been made by Matsuse *et al.*, who proposed a new critical distance model. The solid lines in Fig. 9 are calculated with their model where the parameters given in Ref. 18 are used. The experimental results are better interpreted in terms of the new critical distance model.

At this stage, we can say that the entrance channel plays an important role in fusion reactions at higher energies. The choice of the systems leading to the same compound nucleus with very different entrance channels is sensitive to seeing the difference between the alternative ideas. However, it has been pointed out recently by Morgenstern *et al.*[28] that incomplete fusion reactions contribute strongly at higher incident energies, and that a systematic dependence on the entrance channel asymmetry is observed. The yield of deep-inelastic recoil also starts to mix in the fusion yield in the backward angular region. The case of the $^{12}C+^{50}Cr$ system is the most worrisome because the energy of the evaporation residues is very low. The dotted and the broken lines in Fig. 3(b) show the angular distributions calculated using a Monte-Carlo program called RECOIL.[30] The energy spectrum and the multiplicity of neutrons, protons, and α particles which are estimated by the CASCADE (Ref. 29) program code are used as input data for RECOIL. It is assumed that the angular distribution of each evaporated particle is isotropic around the recoiling nucleus. Though the agreement between the experiment and the calculation is fairly good, a slight difference remains at backward angles. This discrepancy may be due to contributions of processes other than complete fusion. This uncertainty is estimated to be at most about 6%.

As our data contain both complete and incomplete fusion components it appears that the reasonable agreement of the total fusion cross sections with a static model indicates that such a model fails at higher energies, as it should rather give the complete fusion cross section.

V. CONCLUSION

Heavy-ion fusion reactions have been studied for several light-light systems by choosing symmetric and asymmetric systems to form the same compound nucleus. For the systems $^{28}Si+^{28}Si$ and $^{16}O+^{40}Ca$, which form the compound nucleus ^{56}Ni, fusion cross sections were measured in the compound excitation energy range of $E^*=40-85$ MeV. The fusion cross sections in region II for $^{28}Si+^{28}Si$ are well reproduced by the two alternative ideas, the critical distance model and the statistical yrast line model. But those for $^{16}O+^{40}Ca$ are poorly reproduced by both models. On the other hand, the new critical distance model and the Bass model can explain well $\sigma_{fus}^{(II)}$ for the asymmetric system of $^{16}O+^{40}Ca$.

The same features can be seen more dramatically for the systems $^{32}S+^{30}Si$ and $^{12}C+^{50}Cr$, which lead to the compound nucleus ^{62}Zn, in the excitation energy range of $E^*=47-124$ MeV. The results for the very asymmetric systems such as the $^{12}C+^{50}Cr$ system have clearly shown that the entrance channel properties strongly effect the fusion process.

From the present study we conclude that the entrance channel effect like the critical distance plays a significant role in the limitation of fusion cross sections in region II. It appears that the concept of critical distances fails in region III, where significant contributions from incomplete fusion arise.

ACKNOWLEDGMENTS

The authors would like to thank Dr. T. Kishimoto, Dr. T. Matsuse, and Dr. S. Seki for many valuable discussions. We wish to thank the crews of the University of Tsukuba Tandem Accelerator Center and of RCNP of Osaka University. The critical reading of the manuscript by Dr. W. Galster is gratefully acknowledged. This work was supported in part by the Nuclear and Solid State Research Project, University of Tsukuba.

---

*Present address: Institute of Atomic Energy, People's Republic of China.

[1]M. Lefort and Ch. Ngô, Ann. Phys. (N.Y.) 3, 5 (1978); J. R. Huizenga, J. R. Birkelund, W. N. Schröder, W. W. Wilcke, and H. J. Wollersheim, in *Dynamics of Heavy-Ion Collisions, Hvar, 1981,* edited by N. Cindro, R. A. Ricci, and W. Greiner (North-Holland, Amsterdam, 1982), and references therein; S. M. Lee, in Proceedings of the Tsukuba Symposium on Heavy Ion Nuclear Physics, Tsukuba, 1981, edited by T. Kishimoto *et al.*, University of Tsukuba Report NSSRP-44, 1982, p. 55.

[2]J. Galin, D. Guerreau, M. Lefort, and X. Tarrago, Phys. Rev. C 9, 1018 (1974).

[3]D. Glas and U. Mosel, Nucl. Phys. **A237**, 429 (1975).

[4]L. C. Vaz and J. M. Alexander, Phys. Rev. C 18, 2152 (1978).

[5]R. Bass, Phys. Lett. **47B**, 139 (1973).

[6]R. Bass, Nucl. Phys. **A231**, 45 (1974).

[7]R. Bass, Phys. Rev. Lett. **39**, 265 (1977).

[8]D. Horn and A. J. Ferguson, Phys. Rev. Lett. **41**, 1529 (1978).

[9]M. Blann and F. Plasil, Phys. Rev. Lett. **29**, 303 (1972).

[10]W. W. Morrison, S. K. Samaddar, D. Sperber, and Zielinska-Pfabe, Phys. Lett. **99B**, 205 (1981).

[11]D. H. E. Gross and H. Kalinowski, Phys. Lett. **48B**, 302 (1974).

[12]J. R. Birkelund, J. R. Huizenga, J. N. De, and D. Sperber, Phys. Rev. Lett. **40**, 1123 (1978).

[13]K. R. S. Devi, A. K. Dhar, and M. R. Strayer, Phys. Rev. C **23**, 2062 (1981).

[14]P. Bonche, K. T. R. Davies, B. Flanders, H. Flocard, B. Grammaticos, S. E. Koonin, S. J. Krieger, and M. S. Weiss, Phys. Rev. C **20**, 641 (1979).

[15]S. J. Krieger and M. S. Weiss, Phys. Rev C **24**, 928 (1981); H. Lehr *et al.*, Annual Report, Hahn-Meitner-Institute, 1980, p. 67.

[16]S. M. Lee, T. Matsuse, and A. Arima, Phys. Rev. Lett. **45**, 165 (1980).

[17]R. Vandenbosch and A. J. Lazzarini, Phys. Rev. C **23**, 1074 (1981).

[18]T. Matsuse and S. M. Lee, Proceedings of Tsukuba Interna-

tional Symposium on Heavy Ion Fusion Reaction, Tsukuba, 1984.

[19]M. Yamanouchi, Y. Higashi, H. Yamaguchi, and M. Okamoto, Nucl. Instrum. Methods **158**, 339 (1979).

[20]S. Seki, K. Furuno, T. Ishihara, Y. Nagashima, M. Yamanouchi, T. Aoki, T. Mikumo, and J. Sanada, Nucl. Instrum. Methods **184**, 113 (1981).

[21]J. Schimizu and T. Nakagawa, Annual Report, Tandam Accelerator Center, University of Tsukuba, Report UTTAC-40, 1980, p. 29 (unpublished).

[22]S. B. DiCenzo, J. F. Petersen, and R. R. Betts, Phys. Rev. C **23**, 2561 (1981).

[23]D. F. Geesaman, C. N. Davids, W. Henning, D. G. Kovar, K. E. Rehm, J. P. Schiffer, S. L. Tabor, and F. W. Prosser, Jr., Phys. Rev. C **18**, 284 (1978).

[24]S. E. Vigdor, D. G. Kovar, P. Sperr, J. Mahong, A. Menchaca-Rocha, C. Olmer, and M. S. Zisman, Phys. Rev. C **20**, 2147 (1979).

[25]C. Ngô, B. Tamain, J. Galin, M. Beiner, and R. Lombard, Nucl. Phys. **A240**, 353 (1975).

[26]T. Matsuse, A. Arima, T. Tsukamoto, and S. M. Lee, contributed paper in International Conference on Nuclear Physics, Berkeley, 1980, p. 406 (unpublished).

[27]D. G. Kovar, P. D. Bond, C. Flaum, M. J. Levine, and C. E. Thorn, Bull. Am. Phys. Soc. **22**, 66 (1977).

[28]H. Morgenstern, W. Bohne, W. Galster, K. Grabisch, and A. Kyanowski, Phys. Rev. Lett. **52**, 1104 (1984).

[29]F. Puehlhofer, Nucl. Phys. **A280**, 267 (1977).

[30]C. Signorini and G. Fortuna, private communication.